SYNTHESIS AND FLUORESCENCE CHARACTERIZATION OF CARBON QUANTUM DOTS IN TISSUE-MIMICKING PHANTOMS

by

Diyaan Kpanka

A senior thesis submitted to the faculty of

Brigham Young University - Idaho

in partial fulfillment of the requirements for the degree of

Bachelor of Science

Department of Physics

Brigham Young University - Idaho

July 2026

BRIGHAM YOUNG UNIVERSITY - IDAHO

DEPARTMENT APPROVAL

of a senior thesis submitted by

Diyaan Kpanka

This thesis has been reviewed by the research advisor, research coordinator, and department chair and has been found to be satisfactory.

Date	Richard Hatt, Advisor
Date	Cindy Cooper, Committee Member
Date	Todd Lines, Committee Member
Date	Todd Lines, Thesis Coordinator
Date	Evan Hansen, Department Chair

ABSTRACT

SYNTHESIS AND FLUORESCENCE CHARACTERIZATION OF CARBON QUANTUM DOTS IN TISSUE-MIMICKING PHANTOMS

Diyaan Kpanka

Department of Physics

Bachelor of Science

This thesis studies the fluorescence behavior of synthesized carbon quantum dots in tissue-mimicking agarose phantoms. Carbon quantum dots were synthesized from citric acid and urea, excited with a 405 nm source, and analyzed by measuring their emission spectrum, photon energy, Stokes shift, signal attenuation, and detectability through phantoms of increasing thickness. The sample produced a broad fluorescence emission peak near 561 nm. The signal decreased predictably with phantom thickness, following a Beer-Lambert-type attenuation trend while remaining detectable throughout the measured range.

ACKNOWLEDGMENTS

I would like to express my sincere gratitude to Brother Lines, my thesis coordinator, for his guidance, support, and encouragement throughout this project. I would also like to thank Brother Hatt and Brother Hansen for all the advices, feedback, and help they provided me throughout this thesis but also throughout my bachelor's degree. I would also like to thank Sister Nelson and Brother Lemon for their help with the experiments, their practical advice, and their willingness to share their knowledge and time. Their support made an important difference in completing this work.

Finally, I am especially thankful to my wife and my family for their love, patience, encouragement, and constant support. Their belief in me helped me stay motivated and complete this thesis.

Contents

List of Figures

Chapter 1

Introduction

Cancer remains one of the major health problems in modern medicine. In the United States alone, approximately 2,114,850 new cancer cases and 626,140 cancer deaths are projected for 2026 [1]. These numbers show that cancer continues to be a major cause of illness and death, even though major progress has been made in diagnosis, treatment, and survival. The biggest challenge that cancer treatment has been facing reside in early diagnosis and treatment due to high mutation rate and metastasis of cancer cells [2]. Over the past years, there has been several improvements in cancer diagnosis equipment such as computed tomography (CT), magnetic resonance imaging (MRI), positron emission tomography (PET), ultrasound and optical imaging. Although these technologies have greatly improved cancer detection, staging, treatment planning, and patient monitoring, important limitations remain. Some systems are expensive, some have limited sensitivity for very small tumors, and others may have difficulty separating abnormal tissue from normal background tissue [3].

Moreover, radiotherapy and chemotherapy, the typical ways we currently have for treating cancer have been reported to be carrying several serious side effects such as hair loss, neutropenia, blood clotting, death of healthy cells and many more [4][5].

Due to all these complications affiliated with our normal treatment, research has turned to nanoparticles to resolve these majors concerns and over the few years carbon quantum dots especially have gained huge interest in both diagnosis and treatment. These carbon-based nanomaterials offer a safer alternative to conventional quantum dots due to their inherent biocompatibility and low cytotoxicity in biological systems. Furthermore, these nanostructures facilitate the development of innovative nanotheranostic platforms that integrate high-sensitivity bioimaging with targeted drug delivery, thereby minimizing systemic off-target effects. Therefore, because of their fluorescence, biocompatibility, and potential for surface modification, carbon quantum dots are promising materials for biomedical imaging research.

Based on these reasons, our study throughout this paper will be focused on evaluating the fluorescence behavior of synthesized carbon quantum dots in a controlled optical imaging setup. The experiment focuses on measuring how the carbon dots respond to light excitation, identifying their emission peak, and determining whether their fluorescence signal can be detected through agarose phantoms. There is a clear need of furthering the study around carbon dots to know more about their ability specifically on cancer treatment and to be sure of their fluorescence capabilities.

Our first objective is to synthesize the carbon quantum dots and to record their emission spectrum. Using a 420 nm excitation source, the strongest emission should be observed near 540 nm [6], which will be used as the main wavelength for later intensity comparisons.

Our second objective is to calculate the Stokes shift and the photon energy, allowing the confirmation of the presence of actual carbon quantum dots.

The third objective is to study how fluorescence detectability changes when the emitted light passes through agarose phantoms of different thicknesses. Normal studies required the use of actual cell tissue but due to unavailability, the agarose phantoms

give us a controlled way to evaluate fluorescence imaging performance before moving to biological samples or clinical studies in further studies.

The study will include plots of fluorescence intensity versus concentration, fluorescence intensity versus phantom thickness, percent signal loss, and will use the Beer-Lambert law to find the attenuation coefficient of phantoms.

Chapter 2

Background

To fully understand the purpose of this study, it is important to first understand the scientific ideas behind the experiment. This chapter introduces quantum dots, carbon quantum dots, their synthesis, and the importance of agarose phantoms as tissue-mimicking materials for fluorescence measurements.

2.1 Quantum dots

Quantum dots are nanoscale semiconductor particles that have unique optical and electronic properties because of their very small size. Unlike larger bulk materials, quantum dots are small enough for their electrons to be confined in a limited space. This effect, called quantum confinement, changes the way the particles absorb and emit energy. Because of this behavior, quantum dots can absorb light from an excitation source and emit light at a different wavelength when transitioning through their allowed energy levels (Figure 2.1) [7]. This makes them useful for fluorescence-based imaging and sensing applications.

One of the most important features of quantum dots is the tunability of their

fluorescence. Their emission wavelength can be changed by adjusting their size, composition, or surface chemistry. Smaller quantum dots generally emit shorter wavelengths, while larger quantum dots can emit longer wavelengths. This tunability allows quantum dots to produce different colors of light and makes them useful for labeling, imaging, and detecting biological targets. Quantum dots are also known for strong brightness, good photostability, and the ability to support multiplex imaging, where different targets can be labeled with different emission colors [7].

Because of these properties, quantum dots have been widely studied in biomedical research. They have been investigated for bioimaging, biosensing, drug delivery, tissue labeling, and molecular detection and their fluorescence appears to create a measurable optical signal that can help improve contrast and make specific cells, tissues, or biological markers easier to detect [8].

However, traditional semiconductor quantum dots also have important limitations. Many commonly studied quantum dots contain heavy metals such as cadmium, selenium, lead, or mercury. These materials can raise toxicity concerns, especially for biological or clinical applications. For example, cadmium and selenium, which are common components of some quantum dots, are associated with acute and chronic toxicity in living systems [9]. Because of this, safety remains one of the major challenges for the direct use of traditional heavy-metal quantum dots in medicine.

These limitations have encouraged researchers to study safer alternatives, including carbon quantum dots. Carbon quantum dots are carbon-based fluorescent nanoparticles that can keep many useful optical properties of traditional quantum dots while reducing some of the toxicity concerns associated with heavy-metal compositions. They are also attractive because they can be synthesized from low-cost materials, dispersed in water, and modified for biological applications [10]. Their possible use in cancer diagnosis, bioimaging, biosensing, targeted delivery, and ther-

agnostic, has made them an important topic in current oncology-related nanomaterial research.

Figure 2.1 Carbon quantum dots at different wavelengths.

2.2 Carbon Quantum Dots

Carbon quantum dots are a class of fluorescent carbon-based nanomaterials that have gained attention as alternatives to traditional semiconductor quantum dots. Their importance comes not only from their small size and fluorescence, but also from their chemical composition. Since they are mainly carbon-based, they are generally considered more suitable for biological and biomedical studies. Carbon dots are often described as water-soluble, photostable, biocompatible, and easy to functionalize, which makes them useful for live-cell imaging, biosensing, targeted drug delivery, and theragnostic applications [11].

A major advantage of carbon quantum dots is their surface chemistry. The surface of carbon dots usually contains functional groups such as hydroxyl, carboxyl,

and amine groups. These groups help the dots dissolve in water and make it possible to modify their surface for different applications. This is important because surface modification can help carbon dots interact with specific biological targets, carry therapeutic molecules, or improve imaging performance [12].

Carbon quantum dots are also attractive because they can be synthesized using relatively simple and low-cost methods. Many synthesis methods use small organic molecules, polymers, or natural materials as carbon sources. In bottom-up synthesis, carbon dots are formed by heating carbon-rich precursors until carbonization occurs. Citric acid is one of the commonly used carbon sources because it contains reactive carboxyl groups and can form fluorescent carbon structures during heating. The addition of nitrogen-containing compounds, such as urea or ethylenediamine, can improve the photoluminescence properties of the resulting dots by introducing nitrogen-related surface states and changing the electronic structure [11]. They can produce optical signals while also offering possibilities for future surface modification. Recent biomedical reviews describe carbon quantum dots as promising materials for cancer visualization and treatment because of their low cell toxicity, water solubility, tunable fluorescence, and ability to be doped or modified [9,12].

2.3 Carbon Quantum Dots Synthesis

Carbon quantum dots can be synthesized using several different methods, but most approaches are usually grouped into two main categories: top-down synthesis and bottom-up synthesis. In top-down methods, larger carbon materials are broken down into nanoscale particles. In bottom-up methods, small organic molecules are heated or chemically reacted until they form carbonized fluorescent nanoparticles. Both approaches can produce carbon dots, but they differ in cost, equipment needs, reaction

conditions, and control over the final optical properties.

Top-down synthesis (figure 2.2-a) begins with larger carbon structures such as graphite, graphene oxide, carbon nanotubes, or other carbon-rich materials. These materials are cut or broken into smaller nanoscale dots using methods such as laser ablation, arc discharge, electrochemical oxidation, or chemical oxidation. The advantage of top-down synthesis is that it can produce carbon nanostructures from already formed carbon materials. However, these methods often require stronger chemical treatment, special equipment, longer purification steps, or more complex reaction conditions.

Bottom-up synthesis (figure 2.2-b) is different because it starts with small molecular precursors. These molecules are heated, dehydrated, polymerized, and carbonized until carbon dots form. Common carbon sources include citric acid, glucose, carbohydrates, polymers, amino acids, and biomass-derived materials. Bottom-up methods are widely used because they are simple, and low-cost. The bottom-up method also allows control over chemical structure, heteroatom doping, and surface functionality [13].

Several bottom-up techniques have been reported, including hydrothermal synthesis, solvothermal synthesis, microwave-assisted synthesis, thermal decomposition, pyrolysis, and oven heating. Hydrothermal and solvothermal methods usually require sealed reaction vessels where the precursors are heated under pressure. Microwave-assisted synthesis uses microwave energy to heat the reaction mixture quickly and uniformly. Oven or hot-plate heating is simpler and can be used when the goal is to form carbon dots from solid or dissolved precursors without high-pressure equipment [13].

For biomedical and fluorescence imaging studies, bottom-up synthesis is especially useful because it allows the choice of safer and more water-compatible precursors.

Citric acid is one of the most common carbon sources because it is inexpensive, accessible, and can form fluorescent carbon-based products after heating. Nitrogen-containing compounds such as urea, ethylenediamine, or amino acids are often added to improve fluorescence by introducing nitrogen-related surface states. The citric acid/urea system has been widely studied, and the thermal reaction of citric acid and urea can produce a complex mixture of fluorescent molecular species and carbonized particles [6].

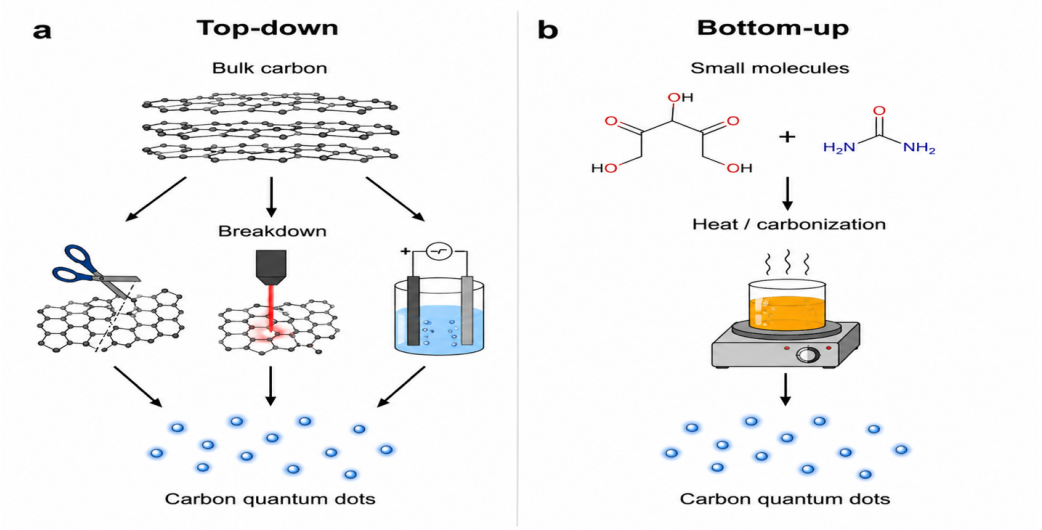

Figure 2.2 Methods of synthesis of carbon quantum dots.

In this project, a bottom-up heating method was selected because it is practical, low-cost, and appropriate for our available laboratory setting. The synthesis uses citric acid as the carbon source and urea as the nitrogen source. The full process of our experiment is described under methods with the specific materials and procedure used to prepare the carbon quantum dots.

2.4 Agarose and its Importance

Agarose is a natural polysaccharide extracted from agar, which comes from red algae. When agarose powder is mixed with water and heated, it dissolves into a liquid solution. As the solution cools, the agarose molecules form a three-dimensional gel network that traps water inside the structure. This produces a soft, clear hydrogel that can hold its shape while still containing a large amount of water.

In biomedical imaging research, agarose is commonly used to prepare tissue-mimicking phantoms. A phantom is a laboratory material designed to imitate selected properties of real tissue. Agarose-based phantoms are useful because their thickness, shape, and composition can be controlled. Agarose-based tissue-mimicking optical phantoms are described as useful models for studying diffuse reflectance and optical properties because they allow researchers to measure how light is absorbed and transmitted through a controlled tissue-like material [14].

For this project, they provide a simple tissue-like medium for studying fluorescence signal loss. When light passes through tissue or a tissue-like phantom, some of the light is absorbed and scattered before reaching the detector. Agarose phantoms allow this effect to be studied safely before using biological tissue. Recent phantom studies show that agarose-based materials can be designed to mimic optical properties of biological tissue, making them useful for light-penetration and biomedical optics experiments [15].

Therefore, Several phantoms of different thicknesses will be prepared, and these phantoms will be placed between the carbon quantum dot sample and the detector to study how the fluorescence signal decreases as the tissue-like layer becomes thicker.

Chapter 3

Methods

This chapter describes the methods used to carry out the experiment. It explains the preparation of the carbon quantum dots, the preparation of the agarose phantoms, and the experimental setup used to collect the fluorescence spectra. These methods provide the foundation for the data analysis presented in the next chapter.

3.1 Carbon dots synthesis (Microwave/Oven Method)

The microwave synthesis method requires simple and accessible materials because it is a bottom-up preparation method. In this experiment, the carbon quantum dots are prepared from a carbon source and a nitrogen source. Citric acid is used as the main carbon source, while urea is used as the nitrogen-containing precursor. During heating, these materials undergo dehydration, polymerization, and carbonization, leading to the formation of fluorescent carbon-based nanoparticles. This method was selected because it required accessible materials, simple equipment, and a short reaction time.

The steps for the whole followed process are described in Figure 3.1.

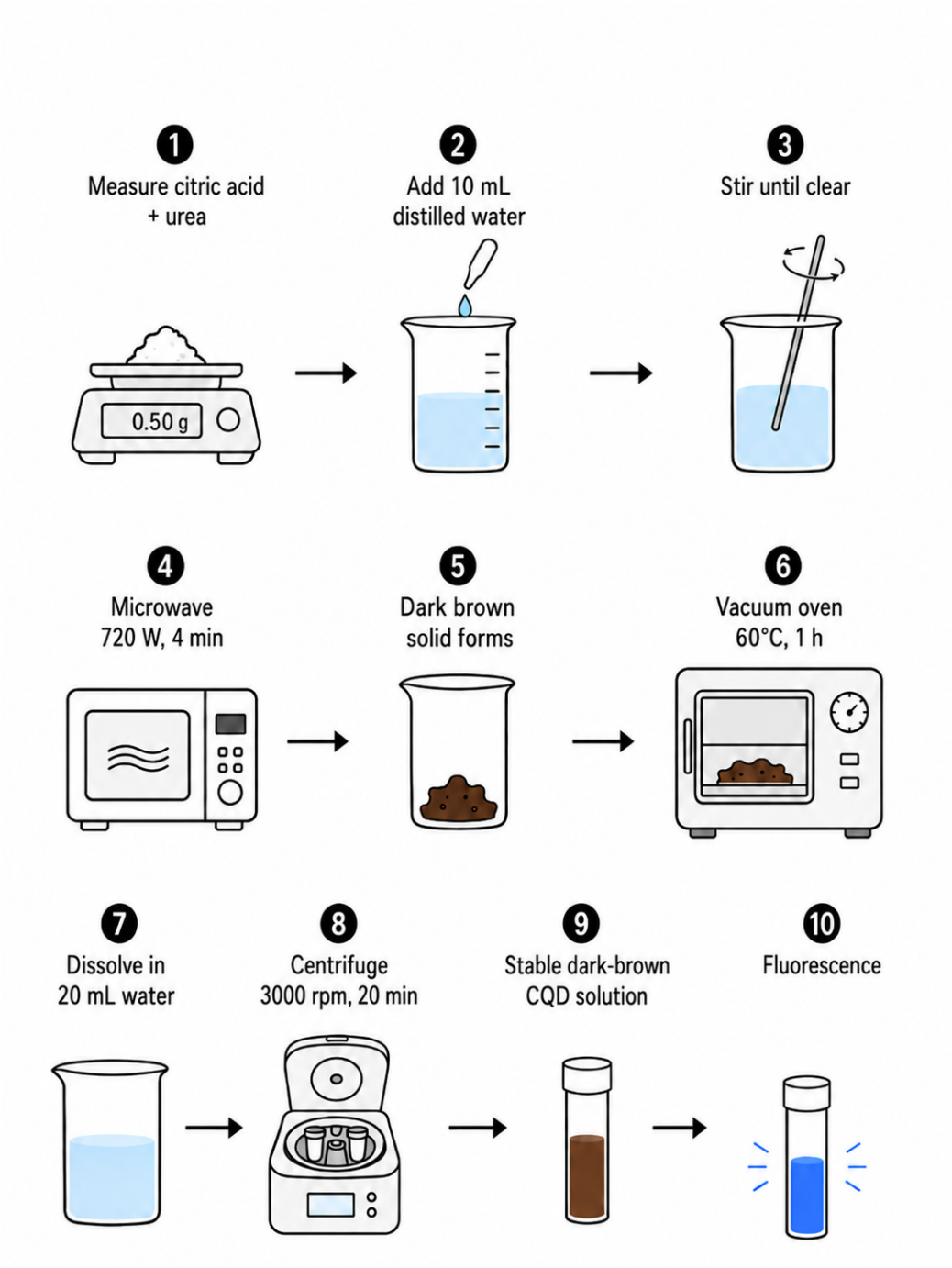

Figure 3.1 Steps of carbon quantum dots preparation using the microwave method.

First, 3.0349 g of citric acid and 3.0337 g of urea were measured and placed into a beaker. Then, 10 mL of pure distilled water was added to the mixture. The solution was stirred with a stirring rod until the solids completely dissolved and the solution became transparent.

After the solution was fully mixed, it was heated in a microwave at 720 W for 4 minutes. During this heating process, the solution changed from transparent to a dark brown solid product. This color change indicated that carbonization had occurred and suggested the formation of carbon quantum dots.

The dark brown product was then transferred to a vacuum oven at 60°C for 1 hour to remove residual small molecules and remaining moisture. After drying, the product was dissolved in 20 mL of pure distilled water to form a carbon quantum dot stock solution.

The solution was then purified using a centrifuge at 3000 rpm for 20 minutes. This step was used to separate larger particles or undissolved material from the carbon dot solution. After centrifugation, the resulting solution had a stable dark brown color (Figure 3.2 a), which was consistent with the formation of carbon quantum dots.

For preliminary fluorescence testing, a small, diluted portion of the carbon dot solution (Figure 3.2 b) was placed under a 365 nm UV light. The sample showed immediate visible fluorescence (Figure 3.2 c), confirming that the synthesized material produced an optical emission response. This fluorescent solution was then used as the stock carbon quantum dot sample for later emission and phantom-thickness measurements [6].

Our expected strongest fluorescence emission in aqueous solution was 540 nm when excited at 420 nm but there was also emission ranging from about 440 nm to 570 nm depending on the excitation wavelength [13].

Our synthesized carbon dots were tested using a 405 nm excitation source, and the

measured emission spectrum showed a peak near 561 nm. This result is reasonably close to the wavelength range reported in [6], especially because their carbon dots also showed emission near 570 nm at higher excitation wavelengths. Therefore, the measured 561 nm peak supports the conclusion that the synthesized sample behaves like fluorescent carbon quantum dots.

3.2 Agarose preparation

For this experiment, a 1.5% agarose phantom was prepared. This concentration was chosen because it produces a gel that is firm enough to hold its shape while still being clear enough for optical measurements. To prepare the phantom, 0.75 g of agarose powder was measured and added to 50 mL of distilled water. This gives a 1.5% mass/volume solution:

The mixture was stirred until the agarose powder was evenly dispersed in the water. It was then heated in a microwave for approximately 40 seconds, or until the solution began to boil and the agarose fully dissolved. Heating was necessary because agarose does not completely dissolve at room temperature. Once heated, the mixture became a clear liquid.

After heating, the hot agarose solution was carefully poured into a container (Figure 3.3 a) or mold (Figure 3.3 b) and allowed to cool at room temperature.

As the solution cooled, it solidified into a gel. The final agarose phantom was transparent to slightly cloudy and firm enough to be handled. The prepared phantom was then used in our setup for fluorescence testing.

The phantom made in the glass container shown in Figure 3.3 b is better for long term use as it allows reduced dehydration. But as the control of the thickness is important, we later opted for the molded version seen in Figure 3.3 b. This version

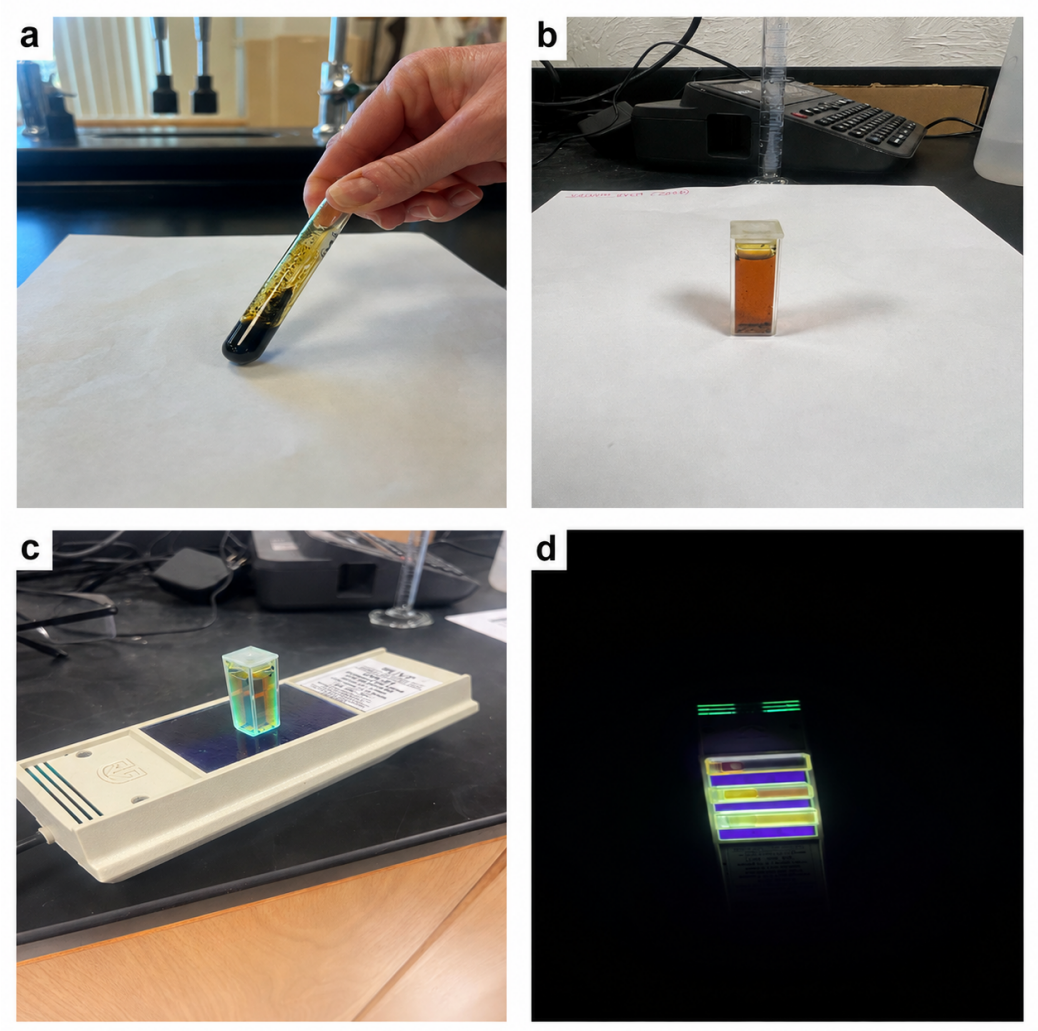

Figure 3.2 Results from the preparation of the carbon quantum dots a) Dark brown solid observed at the bottom of the tube after centrifugation. b) Dilution of small amount of dark solid observed after vacuum oven step for test. c) Test for fluorescence of our sample using a 365 nm UV light revealing the presence of CQD. d) Test of different concentration of resultant product with 365 nm UV light.

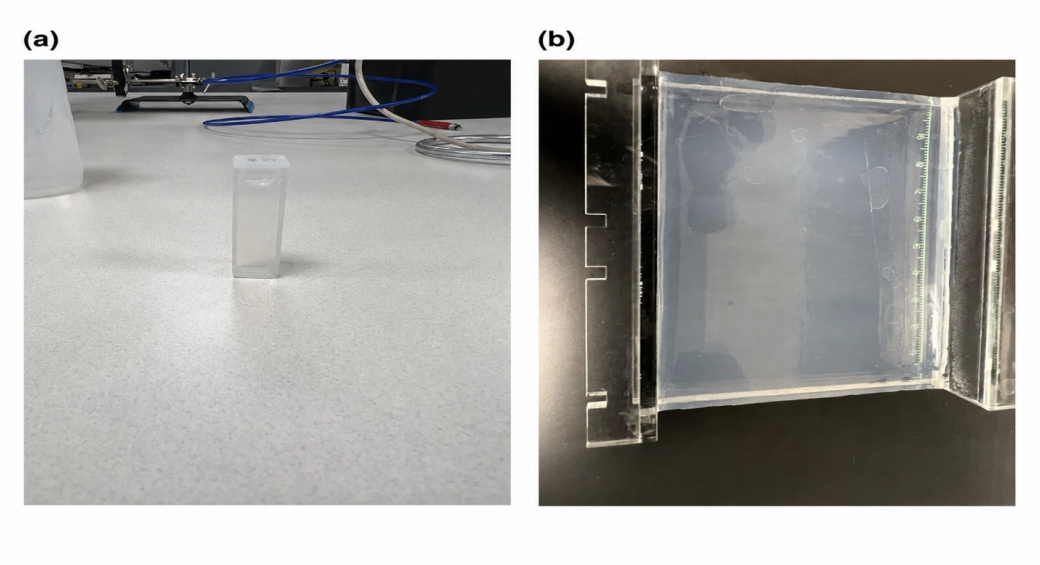

Figure 3.3 a) Agarose phantom conserved in a glass container. b) Agarose phantom made in a mold.

allowed better control and consistency but could only be used for 30 minutes. After 30 minutes, the phantom becomes highly dehydrated, thinner and unreliable. Therefore, our measurements for each phantom were taken within a 30 minutes period.

3.3 Experimental setup

Our experimental setup was designed to keep the measurement conditions as consistent as possible so that changes in intensity could be compared between different samples.

The carbon quantum dot solution was placed in a clear sample glass container and positioned right above the light source. A 405 nm excitation source was used for the emission spectrum measurements. The emitted light was collected using a red tide spectrometer connected to Logger Pro, which recorded intensity as a function of wavelength. We used an optics cable where one end is connected to the red tide spectrometer and the other clamped above the carbon dot sample. It was also necessary

to leave some space between the end of the cable and our sample to make sure we can insert different thicknesses of our agarose phantom.

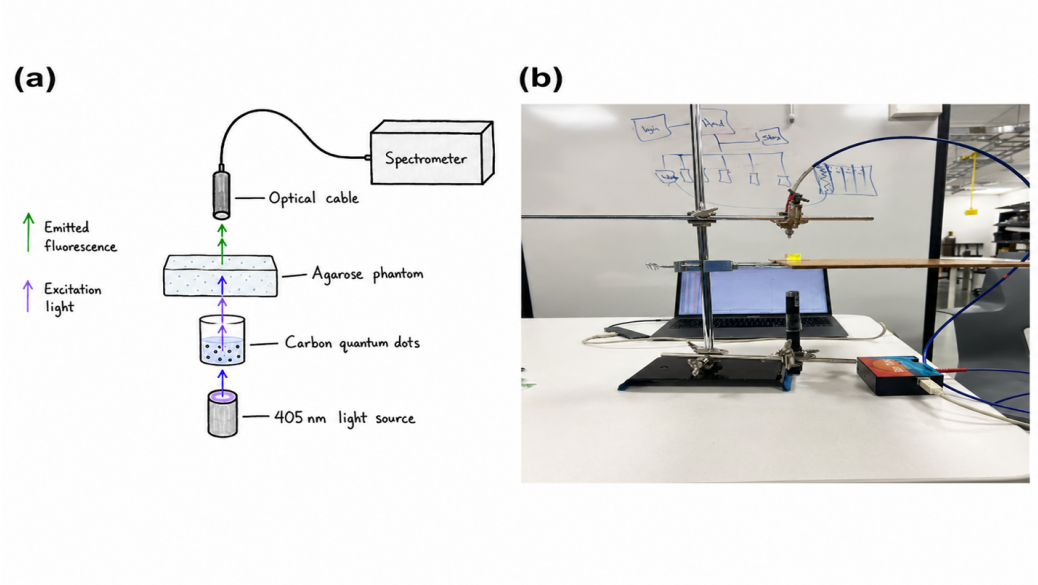

Figure 3.4 a) Design of the experimental setup. b) Experimental setup used for data collection.

All measurements were performed using the same general alignment shown in figure 3.4 a (excitation source, sample, phantom, and detector). We also took the measurements in a dark room to ensure that there was no other light picked up by the detector and avoid changes in distance, angle, or sample position that could affect the measured intensity. The same measurement procedure was used for each trial so that the resulting spectra could be compared fairly.

The data were recorded as intensity (arbitrary units) vs wavelength (nm) and later analyzed by identifying the peak emission wavelength, calculating the Stokes shift and photon energy, comparing intensities, calculating percent signal loss, and applying Beer-Lambert-type attenuation analysis.

Chapter 4

Data Collection and Analysis

The spectra collected during the experiment were analyzed with two goals. The first goal was to confirm that the synthesized sample behaves like fluorescent carbon quantum dots reported by other researchers. The second goal was to measure how well that fluorescence can still be detected after the emitted light passes through a tissue-mimicking agarose phantom. This chapter presents the data extraction method, the emission spectrum, the optical calculations, the blank correction, and the attenuation analysis. Each step builds toward the conclusion that the carbon dots produce a real fluorescence signal and that this signal weakens in a predictable way as phantom thickness increases.

4.1 Data Extraction

The fluorescence spectra were recorded with Logger Pro and saved as .cmbl files. Each file stores the recorded wavelength values and the matching relative intensity values for one measurement. To process many spectra in a consistent way, a short Python program was written to read each .cmbl file, pull out the wavelength and intensity

columns, and convert them into NumPy arrays for plotting and calculation. The full code is given in Appendix C.

The program opens the file, reads its XML structure, and finds the data columns named Wavelength and Intensity. The extracted values are stored as arrays so that every later step (peak finding, blank subtraction, and curve fitting) uses the same clean data set.

4.2 Emission Spectrum and Peak Wavelength

The fluorescence signal only appears at wavelengths longer than the excitation wavelength. Since the excitation source was 405 nm, the emission region of interest is roughly 450 nm to 700 nm. The analysis focused on this region.

Figure 4.1 shows the blank-corrected emission spectrum of the carbon dot sample measured with no phantom in place. The spectrum has one broad band with its maximum near 561 nm. This value is the peak emission wavelength, and it is used as the reference wavelength for every later intensity comparison.

A peak near 561 nm agrees with the range reported for carbon dots made from citric acid and urea, which emit in the green to yellow-green region depending on excitation wavelength [16, 17]. This supports the conclusion that the synthesized sample is fluorescent and behaves like the carbon dots described in the literature.

4.3 Photon Energy and Stokes Shift

The photon energy was calculated to describe the optical transition in energy units. Each wavelength of light carries a fixed amount of energy given by

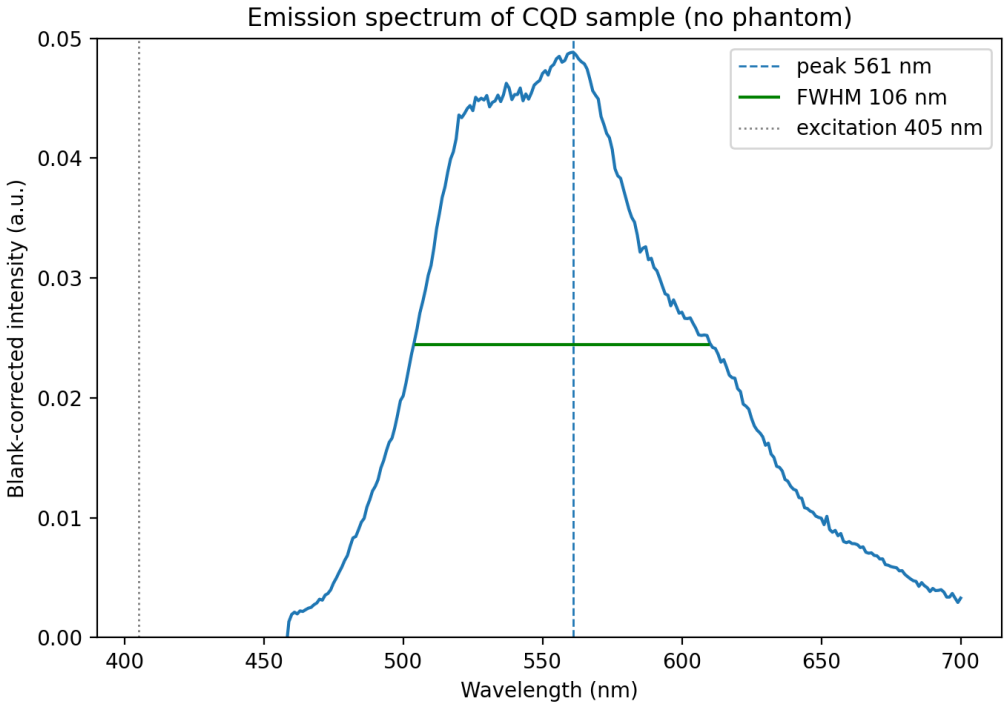

Figure 4.1 Emission spectrum of the carbon dot sample with no phantom, excited at 405 nm. The peak sits near 561 nm and the band are about 106 nm wide at half maximum.

$$E = \frac{hc}{\lambda}. \tag{4.1}$$

where E is the photon energy, h is Planck's constant, c is the speed of light, and λ is the wavelength. When the wavelength is in nanometers and the energy is in electron volts, this becomes

$$E(\text{eV}) = \frac{1240\ \text{eV nm}}{\lambda(\text{nm})}, \tag{4.2}$$

because $hc = 1240$ eV nm. For the 405 nm excitation source,

$$E_{\text{ex}} = \frac{1240\ \text{eV nm}}{405\ \text{nm}} = 3.062\ \text{eV}. \tag{4.3}$$

For the 561 nm emission peak,

$$E_{\text{em}} = \frac{1240\ \text{eV nm}}{561\ \text{nm}} = 2.210\ \text{eV}. \tag{4.4}$$

The energy difference between the absorbed and emitted photon is

$$\Delta E = E_{\text{ex}} - E_{\text{em}} = 0.851\ \text{eV}. \tag{4.5}$$

This result shows that the emitted photon carries less energy than the excitation photon. The missing 0.851 eV is lost through non-radiative relaxation before the photon is emitted. This behavior is the physical meaning of the Stokes shift and confirms that the measured signal is fluorescence, not reflected or scattered excitation light [18].

The Stokes shift can also be written directly. As a wavelength difference,

$$\Delta\lambda = 561\ \text{nm} - 405\ \text{nm} = 156\ \text{nm}. \tag{4.6}$$

A wavelength difference is not linear in energy, so the shift is better reported in wavenumbers,

$$\Delta\tilde{\nu} = \left(\frac{1}{405\text{ nm}} - \frac{1}{561\text{ nm}}\right) 10^7 = 6866\text{ cm}^{-1}. \tag{4.7}$$

Both forms describe the same effect. Because the measurement used a fixed excitation source rather than a measured absorption peak, this quantity is reported as an excitation-to-emission shift.

4.4 Emission Linewidth and Broadening

The width of the emission band carries physical information about the sample. From Figure 4.1, the band is about 106 nm wide at half of its maximum height, spanning roughly 504 nm to 610 nm. Converting these edges to energy using the same calculation process using equation 4.1 gives 2.460 eV and 2.033 eV, so the emission line is about

$$\Delta E_{\text{FWHM}} = 2.460\text{ eV} - 2.033\text{ eV} = 0.428\text{ eV}. \tag{4.8}$$

wide in energy. This width can be compared to the thermal energy available at room temperature,

$$kT \approx 0.0259\text{ eV}. \tag{4.9}$$

The emission width is about 17 times larger than kT. Thermal motion alone cannot broaden a line by that much. The large width therefore comes from inhomogeneous broadening, meaning the sample contains many dots of slightly different size and surface chemistry, each emitting at a slightly different energy [16, 19]. The measured

linewidth is one piece of evidence that the sample is a mixed population rather than a single uniform emitter.

4.5 Background and Blank Correction

The spectrometer collects light from more than the carbon dots alone. It can also pick up the excitation source, the glass container, and the agarose phantom. If these background signals are ignored, the measured intensity would overestimate the true fluorescence. To prevent this, a blank measurement was recorded for each condition and subtracted from the matching sample measurement,

$$I_{\text{corrected}}(\lambda) = I_{\text{sample}}(\lambda) - I_{\text{blank}}(\lambda). \tag{4.10}$$

where I_{sample} is the measured intensity of the carbon dot sample and I_{blank} is the intensity of the matching background. For the no-phantom sample, the UV-only spectrum was used as the blank. For each phantom measurement, the agarose-only spectrum of the same thickness was used as the blank. This matching is important because it removes the background produced by that exact thickness of agarose, so the corrected result reflects only the fluorescence from the carbon dots. In practice the blanks were near zero in the 480 nm to 650 nm region, which confirms that the peak near 561 nm is real fluorescence and not just UV light from excitation.

4.6 Fluorescence Intensity Through Agarose Phantoms

After blank correction, the fluorescence intensity was compared across phantoms of increasing thickness. The comparison used the corrected intensity at the 561 nm

peak. Figure 4.2 overlays the corrected emission spectra for every thickness.

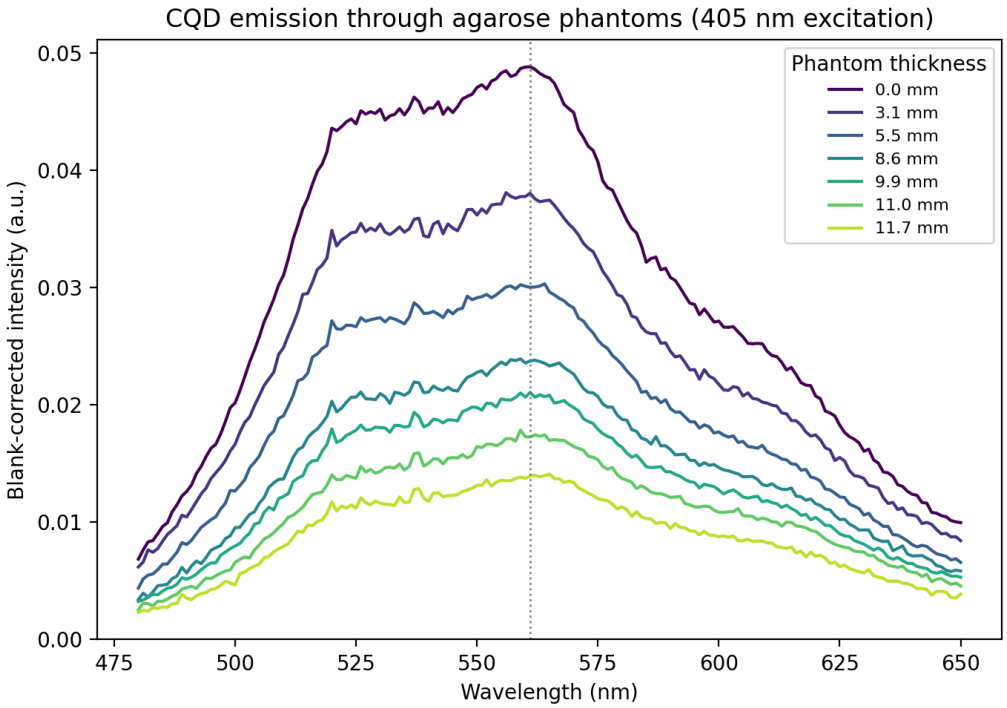

Figure 4.2 Blank-corrected emission spectra through agarose phantoms from 0 mm to 11.7 mm. The dotted line marks 561 nm. The peak drops smoothly as thickness increases.

The peak intensity falls in a smooth and orderly way as the phantom gets thicker. The measured values are listed in Table 4.1.

The intensity drops because the emitted light must travel through more material before reaching the optical cable. As the agarose layer grows, more light is absorbed, scattered, or lost from the collection path, so less signal reaches the detector.

4.7 Percent Signal Loss

To express this decrease as a fraction of the original signal, the percent signal loss was calculated with

Table 4.1 Blank-corrected peak intensity, percent signal remaining, and natural log ratio used for the attenuation fit.

Thickness (mm)	Peak intensity at 561 nm (a.u.)	Signal remaining (%)	$\ln(I_0/I)$
0.0	0.0488	100.0	0.000
3.1	0.0380	77.9	0.250
5.5	0.0300	61.5	0.486
8.6	0.0238	48.6	0.721
9.9	0.0211	43.2	0.840
11.0	0.0173	35.4	1.040
11.7	0.0139	28.6	1.253

$$\% \text{ loss} = 100 \left(1 - \frac{I}{I_0}\right). \tag{4.11}$$

where I_0 is the intensity with no phantom and I is the corrected intensity after the light passes through a phantom. The no-phantom case is the reference, so its loss is set to zero. Figure 4.3 shows the percent of the original signal that still reaches the detector at each thickness.

By 11.7 mm, only about 29 percent of the original signal remains. This shows in plain terms how strongly a tissue-like layer reduces a detectable optical signal.

4.8 Beer-Lambert Attenuation Analysis

The signal loss was described quantitatively with a Beer-Lambert-type model. When light passes through a material, its intensity falls off with distance as

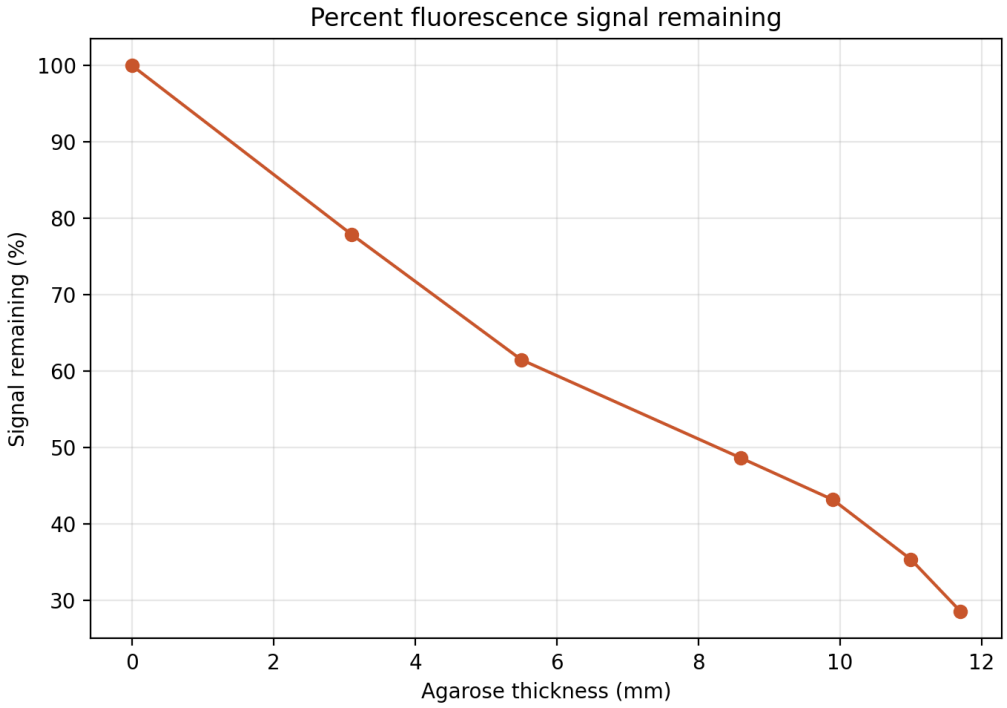

Figure 4.3 Percent of the original fluorescence signal that still reaches the detector as phantom thickness increases.

$$I = I_0 e^{-\mu x}, \tag{4.12}$$

where I_0 is the intensity with no phantom, I is the intensity after a thickness x, and μ is the effective attenuation coefficient [20]. Taking the natural log of both sides makes the relationship linear,

$$\ln\left(\frac{I_0}{I}\right) = \mu x. \tag{4.13}$$

The values of $\ln(I_0/I)$ from Table 4.1 were plotted against thickness. Figure 4.4 shows the raw intensity with its exponential fit, and Figure 4.5 shows the linear form used to extract the slope.

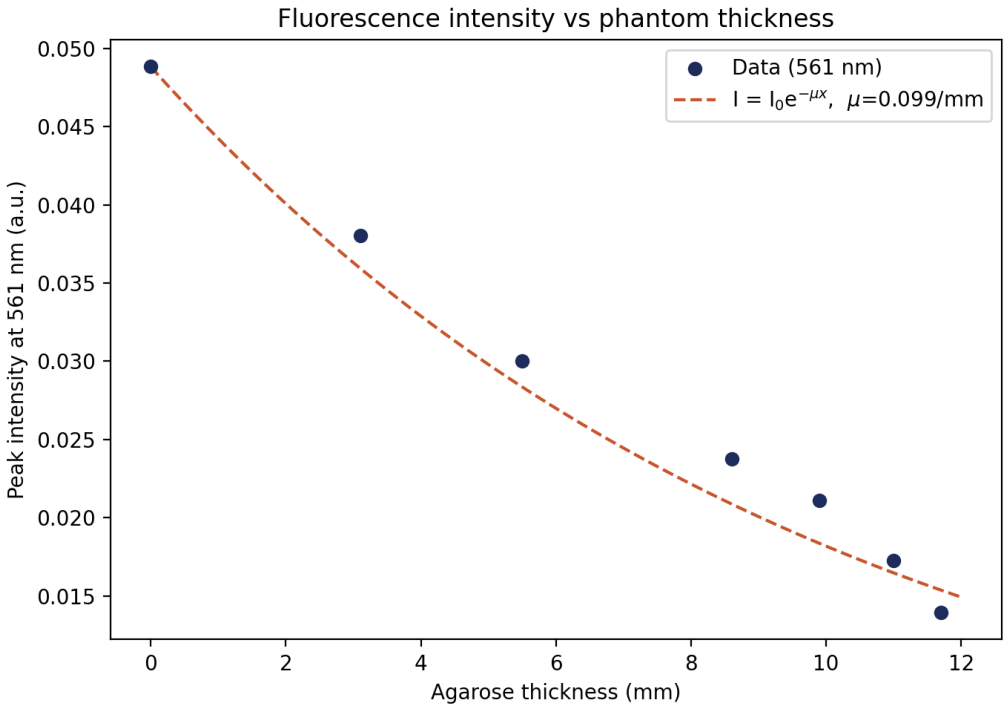

Figure 4.4 Peak intensity at 561 nm versus phantom thickness with an exponential fit.

The linear fit gives an effective attenuation coefficient of

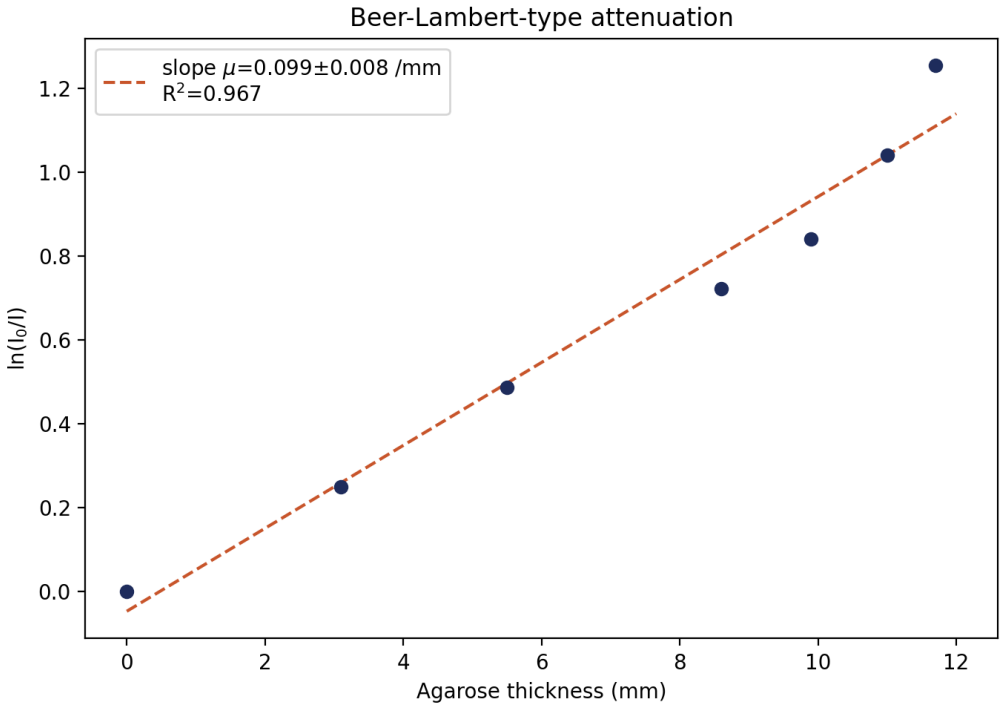

Figure 4.5 Linearized Beer-Lambert plot. The slope is the effective attenuation coefficient.

$$\mu = 0.099 \pm 0.008 \text{ mm}^{-1}, \qquad R^2 = 0.97. \tag{4.14}$$

The fit passes close to the origin, which is expected because there should be no attenuation at zero thickness. The high R^2 and the near-zero intercept both show that the exponential model describes the data fairly well.

Two useful lengths follow directly from μ. The penetration depth is the distance over which the signal falls to $1/e$ of its starting value,

$$\delta = \frac{1}{\mu} = 10.1 \text{ mm}. \tag{4.15}$$

The half-value layer is the thickness that cuts the signal in half,

$$\text{HVL} = \frac{\ln 2}{\mu} = 7.0 \text{ mm}. \tag{4.16}$$

The same attenuation can also be stated as an optical density, $\log_{10}(I_0/I)$, which reaches 0.544 at 11.7 mm.

It is important to interpret μ correctly. Pure water absorbs only about $0.0004\ \text{mm}^{-1}$ near 561 nm [21], so over the full 11.7 mm the water in the gel contributes an absorbance of about 0.005, which is negligible compared to the measured 0.544. The attenuation is therefore not simple molecular absorption. It comes mostly from scattering inside the gel and from light leaving the narrow collection path [22, 23]. For this reason, μ is reported as an effective attenuation coefficient rather than a pure absorption coefficient.

4.9 Reabsorption and Emission Peak Shift

A closer look at the spectra in Figure 4.2 shows a small but consistent change in the shape of the band, not just its height. The center of mass of the emission moves

to longer wavelengths as the phantom gets thicker. Figure 4.6 plots the emission centroid against thickness.

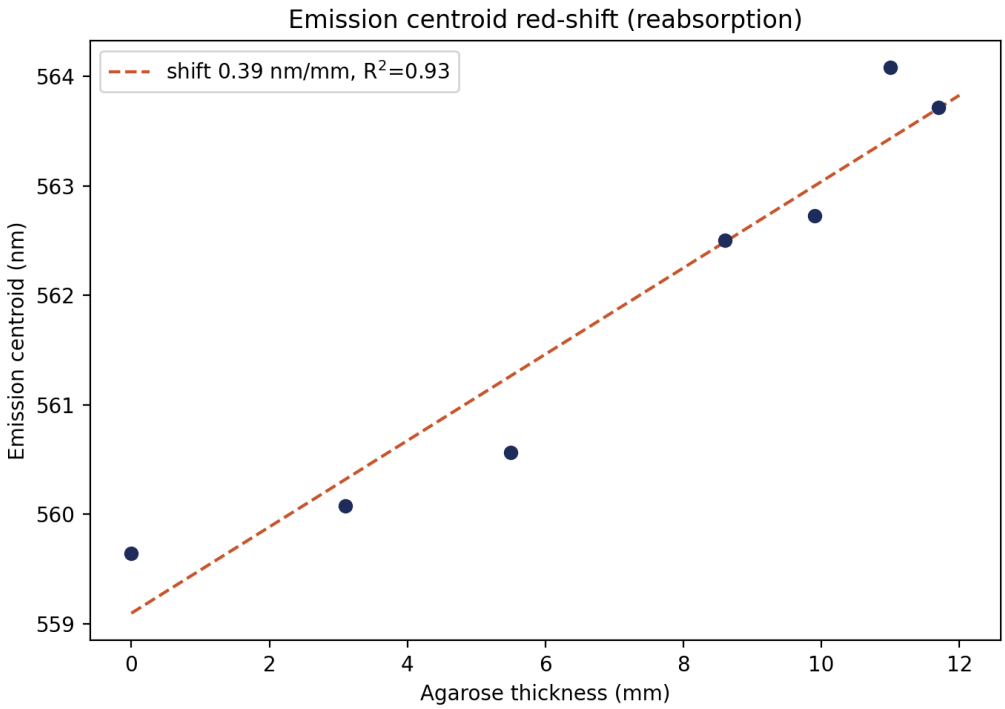

Figure 4.6 Emission centroid versus phantom thickness. The center of the band moves to longer wavelengths as thickness increases.

The centroid moves from about 559.6 nm at 0 mm to about 563.7 nm at 11.7 mm, a red shift of roughly 4 nm at a rate near 0.4 nm per mm. This happens because the shorter-wavelength (higher-energy) side of the emission is absorbed and re-emitted more strongly than the longer-wavelength side as the path length grows. This is a reabsorption or inner-filter effect [18]. It is small here, which is consistent with the large Stokes shift found in Section 4.3, since a large shift means the emission and absorption bands overlap only a little.

4.10 Signal-to-Noise and Detection Limit

The practical question is not only how much signal is lost, but whether the remaining signal can still be distinguished from noise. The noise level was estimated from the standard deviation of a signal-free region of the spectrum (760 nm to 860 nm) after blank correction, giving

$$\sigma = 1.54 \times 10^{-4} \text{ a.u.}. \tag{4.17}$$

The signal-to-noise ratio at the peak was then found for each thickness. It falls from about 317 with no phantom to about 90 at 11.7 mm. Even the thickest phantom leaves the signal far above the noise floor.

Using the exponential model, the thickness at which the signal-to-noise ratio would drop to 3 (a common detection threshold) is

$$x_{\text{SNR}=3} = \frac{\ln(I_0/3\sigma)}{\mu} \approx 39 \text{ mm}. \tag{4.18}$$

This value is an extrapolation well beyond the measured range, so it should be read as a trend estimate rather than a measured result. The single-exponential model will not hold perfectly that far, and the collection geometry will change. Still, the conclusion is clear and useful: across the 0 mm to 12 mm range actually tested, the measurement is not limited by phantom thickness. The signal stays strong. What would limit real imaging is the much higher attenuation of true biological tissue, not the thicknesses used here.

4.11 Summary of Results

The analysis in this chapter supports both goals of the study. Table 4.2 collects the main quantities.

Table 4.2 Summary of the measured and calculated quantities.

Quantity	Symbol	Value
Peak emission wavelength	λ_{peak}	561 nm
Excitation photon energy	E_{ex}	3.062 eV
Emission photon energy	E_{em}	2.210 eV
Energy loss per cycle	ΔE	0.851 eV
Stokes-type shift	$\Delta\lambda$	156 nm (6866 cm^{-1})
Emission linewidth	FWHM	106 nm (0.428 eV)
Effective attenuation coefficient	μ	0.099 ± 0.008 mm^{-1}
Penetration depth	$1/\mu$	10.1 mm
Half-value layer	HVL	7.0 mm
Signal remaining at 11.7 mm	$100I/I_0$	28.6 %
Centroid red shift	$\Delta\lambda_c/\Delta x$	0.4 nm/mm
Peak signal-to-noise (0 mm)	SNR	317

The first goal of this analysis was to confirm that the sample behaves like carbon quantum dots. The emission peak near 561 nm, the Stokes shift of 156 nm, and

the photon energy drops of 0.851 eV all show that the sample absorbs higher-energy light and emits lower-energy light. The broad 0.428 eV linewidth, far larger than the thermal energy, shows the sample is a mixed population of emitters. Together these results confirm that the measured signal is true fluorescence from a carbon-dot-like material.

The second goal was to measure how well that fluorescence survives a tissue-mimicking layer. The intensity falls off exponentially with thickness, with an effective attenuation coefficient of $\mu = 0.099 \pm 0.008$ mm^{-1}, a penetration depth near 10 mm, and a half-value layer of 7 mm. The signal keeps a high signal-to-noise ratio across the full range tested, and the small centroid red shift confirms a weak reabsorption effect. The attenuation is dominated by scattering and collection losses, not by water absorption, which is why the coefficient is treated as effective rather than pure.

Taken together, the data show that the synthesized carbon dots produce a strong, well-behaved fluorescence signal that can be detected through several millimeters of tissue-mimicking material and that weakens in a fairly exponential way with thickness. These findings set up the limitations and future directions discussed in Chapter 5.

Chapter 5

Conclusion and Future Work

Throughout this project, our main goal was to prove that the fluorescence of synthesized carbon dots can be picked up through tissue-mimicking phantoms and to accomplish our goals, multiple process was used.

First the carbon quantum dots were synthesized and analyzed. Throughout the analysis, it was necessary to confirm that the material behaves like a fluorescent carbon dot. Excited at 405 nm, the dots produced one broad emission band peaking near 561 nm. The excitation photon carried 3.062 eV, and the emission photon carried 2.210 eV, a loss of 0.851 eV per cycle, and the excitation-to-emission shift was 156 nm, or 6866 wavenumbers. This energy loss is the defining signature of fluorescence and shows the recorded signal was true emission rather than reflected or scattered excitation light. The emission band was also broad, about 0.428 eV wide, which is roughly 17 times the thermal energy available at room temperature. A width that large cannot come from heat, so it points to a mixed population of dots with a range of sizes and surface states. These results establish that the synthesized sample is truly fluorescent and emits in the green to yellow-green region reported for carbon dots made this way.

Continuing the analysis showed that fluorescence survives a tissue-mimicking layer, which is the central result of the study. As agarose thickness increased, the detected signal fell off smoothly and exponentially. A Beer-Lambert-type fit gave an effective attenuation coefficient of 0.099 ± 0.008 mm^{-1}, with a coefficient of determination of 0.97, matching the exponential model fairly and passing near the origin as expected. From this coefficient the signal has a penetration depth near 10 mm and a half-value layer of about 7 mm, meaning every 7 mm of this material cuts the signal in half. Even through the thickest 11.7 mm phantom, roughly 29 percent of the original signal still reached the detector, and the signal-to-noise ratio stayed strong throughout, falling from about 317 with no phantom to about 90 at the greatest thickness. A small red shift of the emission center, about 4 nm across the full range, revealed a weak reabsorption effect that fits the large Stokes shift found earlier. Because pure water and agarose absorb almost nothing at 561 nm, this attenuation comes mostly from scattering and from light leaving the narrow collection path, so the coefficient is best read as an effective attenuation rather than pure absorption.

Taken together, these findings show that carbon dots produce a strong, stable signal that weakens with distance in a predictable way. That predictability is what makes the material worth carrying forward, because it means the fluorescence can be modeled, corrected and more importantly tracked down.

But the study also sets its limits. The dots were confirmed by how they emit light, not by their structure, since no particle size, absorption spectrum, or quantum yield was measured. So the results describe a fluorescent carbon nanomaterial rather than a fully characterized quantum dot. The agarose phantom captures the geometry of imaging through a layer but is far simpler and more transparent than living tissue, and the visible green emission does not reach as deep as red or near-infrared light so these carbon dots can only be used to target the near skin cells. But these are not

failures and define exactly what must be tested next.

The clearest path forward is to replace the phantom with real animal tissue, starting with a mouse model. The first stage would use ex vivo mouse tissue in the same setup, giving a realistic attenuation value and revealing effects a gel cannot show, such as the tissue's own background glow. The work would then move to living mice, where the dots can be tracked to learn how they spread, where they collect, how long they stay, and how well they can be seen through skin and tissue. This stage would also require safety testing for toxicity and clearance, along with a parallel effort to shift the emission toward the red or near infrared so the signal can be seen from deeper inside the body.

Reaching that point opens the door to theragnostic, where a single particle both finds disease and helps treat it. The imaging behavior measured here is the diagnostic half. The treatment half would be built onto the carbon dots' surface, using targeting molecules to steer them to tumor cells, a drug payload to deliver therapy where the dots light up, or reactive species to destroy nearby cancer cells. In a mouse this could run as a single loop of locating the tumor by its glow, treating that exact spot, and imaging again to watch the response. That is the long-term promise of this work: to turn a simple fluorescent label into a tool that can both see and treat disease. This project confirmed the fluorescence and measured how it fades through tissue-mimicking material, and that is the groundwork on which the rest of that path stands on.

Bibliography

[1] Siegel RL, Kratzer TB, Wagle NS, Sung H, Jemal A. Cancer statistics, 2026. CA Cancer J Clin. 2026;e70043. doi:10.3322/caac.70043.

[2] Sun, S., Klebaner, F., Zhang, X. et al. Instantaneous mutation rate in cancer initiation and progression. BMC Syst Biol 12 (Suppl 6), 110 (2018). https://doi.org/10.1186/s12918-018-0629-z.

[3] Pulumati A, Pulumati A, Dwarakanath BS, Verma A, Papineni RVL. Technological advancements in cancer diagnostics: Improvements and limitations. Cancer Rep (Hoboken). 2023 Feb;6(2):e1764. doi: 10.1002/cnr2.1764. Epub 2023 Jan 6. PMID: 36607830; PMCID: PMC9940009.

[4] PearceA.HaasM.VineyR.PearsonS.HaywoodP.BrownC.et al (2017). Mc Nghim Trng Ca Tc Dng Ph.Pdf, 1–12.

[5] MeirowD.NugentD. (2001). The Effects of Radiotherapy and Chemotherapy on Female Reproduction. Hum. Reprod. Update7, 535–543. 10.1093/humupd/7.6.535.

[6] Qu, S., Wang, X., Lu, Q., Liu, X. and Wang, L. (2012), A Biocompatible Fluorescent Ink Based on Water-Soluble Luminescent Carbon Nanodots. Angew. Chem. Int. Ed., 51: 12215-12218. https://doi.org/10.1002/anie.201206791.

[7] Wagner AM, Knipe JM, Orive G, Peppas NA. Quantum dots in biomedical applications. Acta Biomater. 2019 Aug;94:44-63. doi: 10.1016/j.actbio.2019.05.022. Epub 2019 May 11. PMID: 31082570; PMCID: PMC6642839.

[8] Abdellatif AAH, Younis MA, Alsharidah M, Al Rugaie O, Tawfeek HM. Biomedical Applications of Quantum Dots: Overview, Challenges, and Clinical Potential. Int J Nanomedicine. 2022 May 2;17:1951-1970. doi: 10.2147/IJN.S357980. PMID: 35530976; PMCID: PMC9076002.

[9] Hardman R. A toxicologic review of quantum dots: toxicity depends on physicochemical and environmental factors. Environ Health Perspect. 2006 Feb;114(2):165-72. doi: 10.1289/ehp.8284. PMID: 16451849; PMCID: PMC1367826.

[10] Anand Salvi, Saarthak Kharbanda, Preeti Thakur, Manish Shandilya, Atul Thakur, Biomedical application of carbon quantum dots: A review, Carbon Trends, Volume 17, 2024, 100407, ISSN 2667-0569, https://doi.org/10.1016/j.cartre.2024.100407.

[11] Boakye-Yiadom KO, Kesse S, Opoku-Damoah Y, Filli MS, Aquib M, Joelle MMB, Farooq MA, Mavlyanova R, Raza F, Bavi R, Wang B. Carbon dots: Applications in bioimaging and theranostics. Int J Pharm. 2019 Jun 10;564:308-317. doi: 10.1016/j.ijpharm.2019.04.055. Epub 2019 Apr 20. PMID: 31015004.

[12] Nocito G, Calabrese G, Forte S, Petralia S, Puglisi C, Campolo M, Esposito E, Conoci S. Carbon Dots as Promising Tools for Cancer Diagnosis and Therapy. Cancers (Basel). 2021 Apr 21;13(9):1991. doi: 10.3390/cancers13091991. PMID: 33919096; PMCID: PMC8122497.

[13] Mowery JL, Chen J. Recent Biomedical Applications of Carbon Quantum Dots in Cancer Treatment. J Phys Chem C Nanomater Interfaces. 2024 Oct 3;128(39):16291-16301. doi: 10.1021/acs.jpcc.4c04847. Epub 2024 Sep 20. PMID: 40927338; PMCID: PMC12416908.

[14] Mustari A, Nishidate I, Wares MA, Maeda T, Kawauchi S, Sato S, Sato M, Aizu Y. Agarose-based Tissue Mimicking Optical Phantoms for Diffuse Reflectance Spectroscopy. J Vis Exp. 2018 Aug 22;(138):57578. doi: 10.3791/57578. PMID: 30199019; PMCID: PMC6231702.

[15] Fernandes F, Pereira MRC, Soares D, Fonseca AM, Costa D, Silva FS, Sousa N, Catarino SO, Carvalho . Development and optical characterisation of agarose-based phantoms mimicking biological tissues for studies of light penetration in the brain. Biomater Sci. 2024 Oct 8;12(20):5311-5323. doi: 10.1039/d4bm01044b. PMID: 39248079.

[16] "High quantum yield green-emitting carbon dots for Fe(III) detection, biocompatible fluorescent ink and cellular imaging," Scientific Reports, 2017. [Online]. Available: https://www.ncbi.nlm.nih.gov/pmc/articles/PMC5665951/.

[17] "Synthesis of carbon dots with multiple color emission by controlled graphitization and surface functionalization," 2016. [Online]. Available: https://www.osti.gov/pages/biblio/1469628.

[18] J. R. Lakowicz, Principles of Fluorescence Spectroscopy, 3rd ed. New York, NY, USA: Springer, 2006.

[19] "Carbon dots synthesized from citric acid, urea, and N-methyl-2-pyrrolidone for photoluminescence and electroluminescence," Journal of

Materials Science: Materials in Electronics, 2025. [Online]. Available: https://link.springer.com/article/10.1007/s10854-025-15834-4.

[20] S. L. Jacques, "Optical properties of biological tissues: a review," Physics in Medicine and Biology, vol. 58, no. 11, pp. R37–R61, 2013.

[21] G. M. Hale and M. R. Querry, "Optical constants of water in the 200-nm to 200-um wavelength region," Applied Optics, vol. 12, no. 3, pp. 555–563, 1973.

[22] M. Lualdi, A. Colombo, B. Farina, S. Tomatis, and R. Marchesini, "A phantom with tissue-like optical properties in the visible and near infrared for use in photomedicine," Lasers in Surgery and Medicine, vol. 28, no. 3, pp. 237–243, 2001.

[23] "Agarose and Intralipid tissue-mimicking phantom for optical coherence tomography," 2016. [Online]. Available: https://arxiv.org/abs/1610.01658.

Appendix A

Lists of Materials Used for Carbon Quantum Dots Synthesis

A.1 Chemicals and Reagents

A.2 Glassware and Lab Supplies

A.3 Equipment

Table A.1 Chemicals and Reagents

Material	Amount Used	Purpose
Citric acid	3.0349 g	Carbon source for carbon quantum dot synthesis
Urea	3.0337 g	Nitrogen source and surface passivation agent
Distilled water	10 mL	Used to dissolve citric acid and urea before microwave heating
Distilled water	20 mL	Used to redissolve the synthesized carbon dot product after drying

Table A.2 Glassware and Lab Supplies

Material	Purpose
Beaker	Used to mix citric acid, urea, and distilled water
Stirring rod	Used to stir the solution until fully dissolved
Pipette or dropper	Used to transfer small amounts of solution
Centrifuge tubes	Used during purification of the carbon dot solution
Sample vial or container	Used to store the final carbon quantum dot solution

Table A.3 Equipment

Equipment	Purpose
Analytical balance	Used to measure citric acid and urea
Microwave	Used to heat the precursor solution at 720 W for 4 minutes
Vacuum oven	Used to dry the dark brown product at 60°C for 1 hour
Centrifuge	Used to purify the carbon dot solution at 3000 rpm for 20 minutes
365 nm UV lamp	Used for preliminary fluorescence testing

Appendix B

Lists of Materials Used for Agarose Phantoms Preparation

B.1 Chemicals and Reagents

Table B.1 Chemicals and Reagents

Material	Amount Used	Purpose
Agarose powder	0.75 g	Used to form the tissue-mimicking gel phantom
Distilled water	50 mL	Used to dissolve the agarose powder

B.2 Lab Supplies

B.3 Equipment

Table B.2 Lab Supplies

Material	Purpose
Beaker	Used to mix the agarose powder and distilled water
Stirring rod	Used to stir the agarose mixture before heating
Mold or small container	Used to shape the agarose phantom while it cooled and solidified
Ruler or caliper	Used to measure the thickness of the agarose phantoms
Gloves	Used for safe handling of the hot agarose solution and lab materials

Table B.3 Equipment

Equipment	Purpose
Analytical balance	Used to measure 0.75 g of agarose powder
Microwave	Used to heat the agarose mixture until boiling and fully dissolved

Appendix C

Full Python Code

```
"""
Fluorescence␣Analysis
"""
import xml.etree.ElementTree as ET
import numpy as np
from scipy import stats
import matplotlib
matplotlib.use("Agg")          # save figures without opening a
    window
import matplotlib.pyplot as plt
#
    ----------------------------------------------------------------------

# Constants
#
    ----------------------------------------------------------------------

HC = 1240.0 # h*c in eV*nm,
KT_300 = 0.02585 # thermal energy k_B * T at 300 K, in eV
EMISSION_LO = 480 # lower edge of the emission analysis window, in
    nm
EMISSION_HI = 650 # upper edge of the emission analysis window, in
    nm
EXCITATION = 405 # excitation source wavelength, in nm
#
    ----------------------------------------------------------------------

# Data extraction
#
    ----------------------------------------------------------------------

def read_cmbl(file_path):
```

```
"""
Read one Logger Pro .cmbl file and return its wavelength and
intensity data as NumPy arrays.
"""
tree = ET.parse(file_path) # open and parse the XML
root = tree.getroot()
wavelength = None
intensity = None
# Loop over every DataColumn element
for data_column in root.findall(".//DataColumn"):
name = data_column.findtext("DataObjectName")
cells = data_column.findtext("ColumnCells")
# Skip a column that is missing its name
if name is None or cells is None:
continue
# The numbers are stored as space-separated text. Convert each
# to a float and skip anything that is not a number.
values = []
for value in cells.split():
try:
values.append(float(value))
except ValueError:
pass
if name == "Wavelength":
wavelength = np.array(values)
elif name == "Intensity":
intensity = np.array(values)
return wavelength, intensity
def intensity_only(file_path):
"""Return just the intensity array from a file."""
return read_cmbl(file_path)[1]
# Every carbon dot measurement is paired with the blank of the same
PAIRS = {
0.0:  ("UV-CQD.cmbl",          "UV only.cmbl"),
3.1:  ("UV-3.1mmAgar-CQD.cmbl", "UV-3.1mm Agar.cmbl"),
5.5:  ("UV-5.5mmAgar-CQD.cmbl", "UV-5.5mmAgar.cmbl"),
8.6:  ("UV-8.6mmAgar-CQD.cmbl", "UV-8.6mmAgar.cmbl"),
9.9:  ("UV-9.9mmAgar-CQD.cmbl", "UV-9.9mmAgar.cmbl"),
11.0: ("UV-11mmAgar-CQD.cmbl",  "UV-11mmAgar.cmbl"),
11.7: ("UV-11.7mmAgar-CQD.cmbl", "UV-11.7mmAgar.cmbl"),
}
WAVELENGTH, _ = read_cmbl("UV-CQD.cmbl")
# select the emission
EM_MASK = (WAVELENGTH >= EMISSION_LO) & (WAVELENGTH <= EMISSION_HI)
EM_WL = WAVELENGTH[EM_MASK]
def corrected_spectrum(thickness):
"""Blank-corrected spectrum (sample minus matching blank)."""
sample_file, blank_file = PAIRS[thickness]
return intensity_only(sample_file) - intensity_only(blank_file)
#
    ----------------------------------------------------------------------
```

```
# Emission spectrum and peak wavelength
#
    ------------------------------------------------------------------------

# no-phantom sample as reference
reference = corrected_spectrum(0.0)
reference_em = reference[EM_MASK]
# The peak emission wavelength
peak_index_em = np.argmax(reference_em)
PEAK_WL = EM_WL[peak_index_em]
# Index of the peak wavelength on the full wavelength axis
# intensity comparisons are taken wavelength
PEAK_INDEX = np.argmin(np.abs(WAVELENGTH - PEAK_WL))
print(f"Peak␣emission␣wavelength:␣{PEAK_WL:.0f}␣nm")
print(f"Peak␣intensity:␣␣␣␣{reference[PEAK_INDEX]:.4f}␣a.u.")
#
    ------------------------------------------------------------------------

# Photon energy and Stokes shift
#
    ------------------------------------------------------------------------

E_ex = HC / EXCITATION  # excitation photon energy
E_em = HC / PEAK_WL  # emission photon energy
delta_E = E_ex - E_em   # energy lost per cycle
stokes_nm = PEAK_WL - EXCITATION
# Shift in wavenumbers.
stokes_cm = (1.0 / EXCITATION - 1.0 / PEAK_WL) * 1e7
print(f"E_ex␣=␣{E_ex:.3f}␣eV,␣␣E_em␣=␣{E_em:.3f}␣eV,␣␣dE␣=␣{delta_E
    :.3f}␣eV")
print(f"Stokes␣shift␣=␣{stokes_nm:.0f}␣nm␣=␣{stokes_cm:.0f}␣cm^-1␣=␣
    {delta_E:.3f}␣eV")
#
    ------------------------------------------------------------------------

# Emission linewidth and broadening
#
    ------------------------------------------------------------------------

# Full width at half maximum
half_max = reference_em.max() / 2.0
above_half = EM_WL[reference_em >= half_max]
fwhm_nm = above_half.max() - above_half.min()
# Convert the two half-max edges to energy
E_high = HC / above_half.min()
E_low = HC / above_half.max()
fwhm_eV = E_high - E_low
print(f"FWHM␣=␣{fwhm_nm:.0f}␣nm␣({above_half.min():.0f}␣to␣{
    above_half.max():.0f}␣nm)")
print(f"FWHM␣in␣energy␣=␣{fwhm_eV:.3f}␣eV")
```

```
print(f"FWHM␣/␣kT␣=␣{fwhm_eV␣/␣KT_300:.0f}␣␣␣(>>␣1␣means␣broadening␣
    is␣not␣thermal)")
#
    ------------------------------------------------------------------------

# Blank-corrected intensity through phantoms
#
    ------------------------------------------------------------------------

# Build the main results table: for each thickness collect the peak
# intensity and the integrated area of the emission band.
thicknesses = np.array(sorted(PAIRS))
peak_intensity = []
band_area = []
for x in thicknesses:
corr = corrected_spectrum(x)
peak_intensity.append(corr[PEAK_INDEX])
# Integrate the emission band. Clip negatives so noise below zero
# does not subtract from the area.
band = np.clip(corr[EM_MASK], 0, None)
band_area.append(np.trapezoid(band, EM_WL))
peak_intensity = np.array(peak_intensity)
band_area = np.array(band_area)
I0_peak = peak_intensity[0]
I0_area = band_area[0]
print(f"{'x(mm)':>6}{'I_peak':>10}{'%remain':>10}{'ln(I0/I)':>10}")
for x, Ipk in zip(thicknesses, peak_intensity):
pct = 100 * Ipk / I0_peak
ln_ratio = np.log(I0_peak / Ipk)
print(f"{x:6.1f}{Ipk:10.4f}{pct:10.1f}{ln_ratio:10.3f}")
#
    ------------------------------------------------------------------------

# Percent signal loss
#
    ------------------------------------------------------------------------

percent_remaining = 100 * peak_intensity / I0_peak
percent_loss = 100 - percent_remaining
#
    ------------------------------------------------------------------------

# Beer-Lambert attenuation analysis
#
    ------------------------------------------------------------------------

# ln(I0 / I) = mu * x
ln_ratio_peak = np.log(I0_peak / peak_intensity)
mu, intercept, r_value, p_value, mu_se = stats.linregress(
thicknesses, ln_ratio_peak)
# Cross-check the same fit on the integrated band area
```

```
ln_ratio_area = np.log(I0_area / band_area)
mu_area, intercept_a, r_area, p_a, se_a = stats.linregress(
thicknesses, ln_ratio_area)
penetration_depth = 1.0 / mu
half_value_layer = np.log(2) / mu
optical_density = np.log10(I0_peak / peak_intensity[-1])  # at max
    thickness
print(f"mu (peak) = {mu:.4f} +/- {mu_se:.4f} /mm,  R^2 = {r_value
    **2:.3f}")
print(f"mu (area) = {mu_area:.4f} /mm,  R^2 = {r_area**2:.3f}  (
    cross-check)")
print(f"Penetration depth 1/mu = {penetration_depth:.1f} mm")
print(f"Half-value layer ln2/mu = {half_value_layer:.1f} mm")
print(f"Optical density at {thicknesses[-1]:.1f} mm = {
    optical_density:.3f}")
# Water absorbs only about 0.0004 /mm at 561 nm, so over the full
    path
# its absorbance is negligible compared with the measured value.
print(f"Water absorbance over {thicknesses[-1]:.1f} mm ~ "
f"{0.0004 * thicknesses[-1]:.4f} (negligible)")
#
    ---------------------------------------------------------------------

# Reabsorption and emission peak shift
#
    ---------------------------------------------------------------------

# Track the centroid (center of mass) of the emission band
centroids = []
for x in thicknesses:
band = np.clip(corrected_spectrum(x)[EM_MASK], 0, None)
centroids.append(np.sum(EM_WL * band) / np.sum(band))
centroids = np.array(centroids)
shift_slope, shift_int, shift_r, shift_p, shift_se = stats.
    linregress(
thicknesses, centroids)
print(f"Centroid at 0 mm:     {centroids[0]:.1f} nm")
print(f"Centroid at {thicknesses[-1]:.1f} mm: {centroids[-1]:.1f} nm
    ")
print(f"Red shift = {centroids[-1] - centroids[0]:.1f} nm "
f"({shift_slope:.2f} nm/mm,  R^2 = {shift_r**2:.2f})")
#
    ---------------------------------------------------------------------

# Signal-to-noise and detection limit
#
    ---------------------------------------------------------------------

# Estimate noise from a signal-free region of the reference spectrum
    .
noise_mask = (WAVELENGTH >= 760) & (WAVELENGTH <= 860)
```

```
sigma = np.std(reference[noise_mask])
snr = peak_intensity / sigma
# Thickness where the modeled signal would fall to SNR = 3.
detection_limit = np.log(I0_peak / (3 * sigma)) / mu
print(f"Noise sigma = {sigma:.5f} a.u.")
print(f"SNR at 0 mm = {snr[0]:.0f},  SNR at {thicknesses[-1]:.1f} mm
    = {snr[-1]:.0f}")
print(f"Predicted SNR=3 detection limit = {detection_limit:.0f} mm (
    extrapolated)")
#
    ----------------------------------------------------------------------

# Plotting
#
    ----------------------------------------------------------------------

def figure_reference_peak():
""" reference emission spectrum with peak and FWHM."""
wide = (WAVELENGTH >= 450) & (WAVELENGTH <= 700)
w, s = WAVELENGTH[wide], reference[wide]
plt.figure(figsize=(7, 5))
plt.plot(w, s, lw=1.5)
plt.axvline(PEAK_WL, ls="--", lw=1, label=f"peak {PEAK_WL:.0f} nm")
plt.hlines(half_max, above_half.min(), above_half.max(),
color="green", lw=1.5, label=f"FWHM {fwhm_nm:.0f} nm")
plt.axvline(EXCITATION, ls=":", c="gray", lw=1,
label=f"excitation {EXCITATION} nm")
plt.xlabel("Wavelength (nm)")
plt.ylabel("Blank-corrected intensity (a.u.)")
plt.title("Emission spectrum of CQD sample (no phantom)")
plt.legend()
plt.tight_layout()
plt.savefig("fig_reference_peak.png", dpi=200)
plt.close()
def figure_emission_overlay():
""" emission spectra through all phantom thicknesses."""
colors = plt.cm.viridis(np.linspace(0, 0.9, len(thicknesses)))
plt.figure(figsize=(7, 5))
for x, col in zip(thicknesses, colors):
plt.plot(EM_WL, corrected_spectrum(x)[EM_MASK],
color=col, label=f"{x:.1f} mm")
plt.axvline(PEAK_WL, ls=":", c="gray", lw=1)
plt.xlabel("Wavelength (nm)")
plt.ylabel("Blank-corrected intensity (a.u.)")
plt.title("CQD emission through agarose phantoms (405 nm excitation)
    ")
plt.legend(title="Phantom thickness", fontsize=8)
plt.tight_layout()
plt.savefig("fig_emission_overlay.png", dpi=200)
plt.close()
def figure_percent_remaining():
```

```
"""percent␣of␣the␣signal␣that␣still␣reaches␣the␣detector."""
plt.figure(figsize=(7, 5))
plt.plot(thicknesses, percent_remaining, "o-")
plt.xlabel("Agarose␣thickness␣(mm)")
plt.ylabel("Signal␣remaining␣(%)")
plt.title("Percent␣fluorescence␣signal␣remaining")
plt.tight_layout()
plt.savefig("fig_percent_remaining.png", dpi=200)
plt.close()
def figure_intensity_decay():
"""␣peak␣intensity␣versus␣thickness␣with␣exponential␣fit."""
plt.figure(figsize=(7, 5))
plt.scatter(thicknesses, peak_intensity, zorder=3,
label=f"Data␣({PEAK_WL:.0f}␣nm)")
xf = np.linspace(0, thicknesses.max() + 0.5, 100)
plt.plot(xf, I0_peak * np.exp(-mu * xf), "--",
label=fr"$I␣=␣I_0␣e^{{-\mu␣x}}$,␣␣$\mu$={mu:.3f}/mm")
plt.xlabel("Agarose␣thickness␣(mm)")
plt.ylabel(f"Peak␣intensity␣at␣{PEAK_WL:.0f}␣nm␣(a.u.)")
plt.title("Fluorescence␣intensity␣vs␣phantom␣thickness")
plt.legend()
plt.tight_layout()
plt.savefig("fig_intensity_decay.png", dpi=200)
plt.close()
def figure_beer_lambert():
"""␣linearized␣Beer-Lambert␣plot."""
plt.figure(figsize=(7, 5))
plt.scatter(thicknesses, ln_ratio_peak, zorder=3)
xf = np.linspace(0, thicknesses.max() + 0.5, 100)
plt.plot(xf, mu * xf + intercept, "--",
label=f"slope␣$\\mu$={mu:.3f}$\\pm${mu_se:.3f}␣/mm\n"
f"R$^2$={r_value**2:.3f}")
plt.xlabel("Agarose␣thickness␣(mm)")
plt.ylabel(r"ln(I$_0$/I)")
plt.title("Beer-Lambert-type␣attenuation")
plt.legend(loc="upper␣left")
plt.tight_layout()
plt.savefig("fig_beerlambert.png", dpi=200)
plt.close()
def figure_centroid_shift():
"""␣emission␣centroid␣red-shift␣with␣thickness."""
plt.figure(figsize=(7, 5))
plt.scatter(thicknesses, centroids, zorder=3)
xf = np.linspace(0, thicknesses.max() + 0.5, 50)
plt.plot(xf, shift_slope * xf + shift_int, "--",
label=f"shift␣{shift_slope:.2f}␣nm/mm,␣R$^2$={shift_r**2:.2f}")
plt.xlabel("Agarose␣thickness␣(mm)")
plt.ylabel("Emission␣centroid␣(nm)")
plt.title("Emission␣centroid␣red-shift␣(reabsorption)")
plt.legend()
plt.tight_layout()
```

```
plt.savefig("fig_centroid_shift.png", dpi=200)
plt.close()
def make_all_figures():
"""Generate␣and␣save␣every␣figure␣used␣in␣Chapter␣4."""
figure_reference_peak()
figure_emission_overlay()
figure_percent_remaining()
figure_intensity_decay()
figure_beer_lambert()
figure_centroid_shift()
print("\nSaved␣6␣figures.")
if __name__ == "__main__":
make_all_figures()
```